NRIAG Journal of Astronomy and Geophysics (2014) 3, 170–183

National Research Institute of Astronomy and Geophysics

NRIAG Journal of Astronomy and Geophysics

www.elsevier.com/locate/nrjag

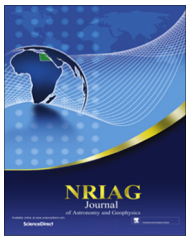

Subsurface investigation on Quarter 27 of May 15th city, Cairo, Egypt using electrical resistivity tomography and shallow seismic refraction techniques

Sultan Awad Sultan Araffa *, Magdy A. Atya, Adel M.E. Mohamed, Mahmoud Gabala, Mohamed Abdel Zaher, Mamdouh M. Soliman, Hany S. Mesbah, Usama Massoud, Hany M. Shaaban

National Research Institute of Astronomy and Geophysics (NRIAG), 11421 Helwan, Cairo, Egypt

Received 20 May 2014; revised 29 September 2014; accepted 14 October 2014
Available online 26 November 2014

KEYWORDS

Quarter 27;
ERT;
Seismic refraction;
MASW;
Structures and construction

Abstract Geophysical tools such as electrical resistivity tomography (ERT) and shallow seismic (both P-wave seismic refraction and Multi-channel Analysis of Surface Waves (MASW)) are interesting techniques for delineating the subsurface configurations as stratigraphy, structural elements, caves and water saturated zones. The ERT technique is used to delineate the contamination, to detect the buried objects, and to quantify some aquifer properties. Eight 2-D (two dimensional) electrical resistivity sections were measured using two different configurations (dipole–dipole and Wenner). The spread length is of 96 m and the electrodes spacing are 2, 4 and 6 m, respectively to reach a depth ranging from 13 to 17 m. The results indicate that, the subsurface section is divided into main three geo-electrical units, the first is fractured marl and limestone which exhibits high resistivity values ranging from 40 to 300 ohm m. The second unit is corresponding to marl of moderate resistivity values and the third unit, which is the deeper unit, exhibits very low resistivity values corresponding to clayey marl. The fourth layer is marly clay with water. The presence of clay causes the most geotechnical problems. Fourteen shallow seismic sections (both for P-wave and MASW) were carried out using spread of 94 m and geophone spacing of 2 m for each P-wave section. The results demonstrate that the deduced subsurface section consists of four layers, the first layer exhibits very low P-wave velocity ranging from 280 to 420 m/s, the second layer reveals P-wave velocity ranging from 400 to 1200 m/s, the third layer has P-wave velocity ranging from 970 to 2000 m/s and

* Corresponding author.

Peer review under responsibility of National Research Institute of Astronomy and Geophysics.

ELSEVIER Production and hosting by Elsevier

http://dx.doi.org/10.1016/j.nrjag.2014.10.004

the fourth layer exhibits high velocity ranging from 1900 to 3600 m/s. The ERT and shallow seismic results, reflect the presence of two parallel faults passing through Quarter 27 and trending NW-SE.

1. Introduction

In the last few years, the application of geophysics in civil and environmental engineering has been become a promising approach. Geophysical tools are implemented in a wide range of applications ranging from building ground investigations to the inspection of dams and dikes (Klimis et al., 1999; Luna and Jadi, 2000; Othman, 2005; Savvaidis et al., 1999; Soupios et al.,

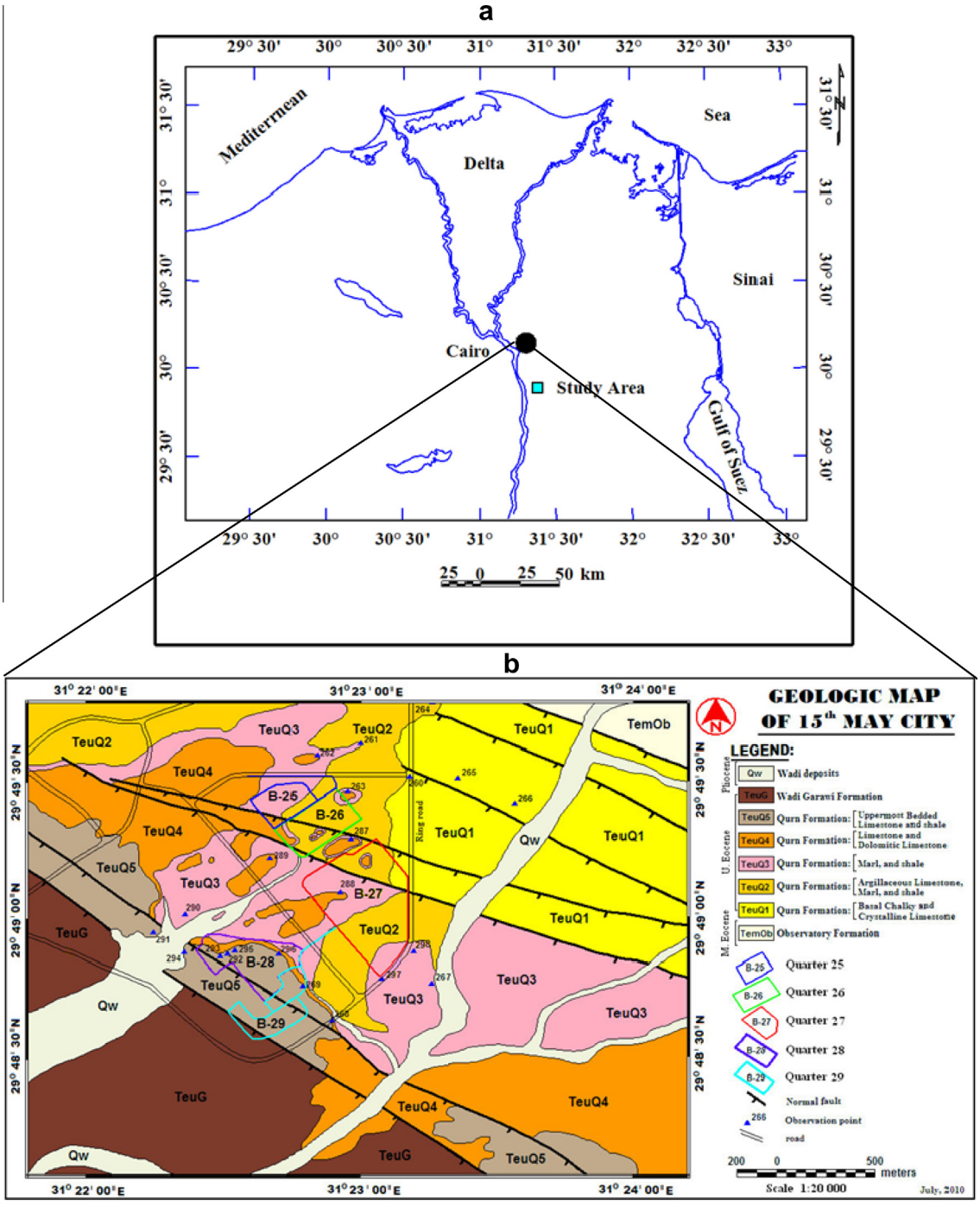

Fig. 1 (a) Location map. (b) Geological map of the study area.

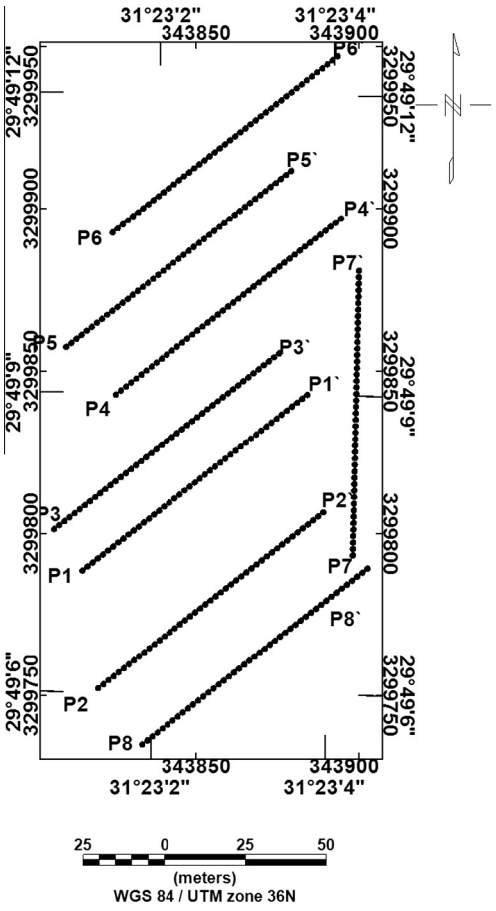

Fig. 2 Location map of the electrical resistivity sections.

2006 and Venkateswara et al., 2004), aiming toward the exploration of geological and the determination of the physical parameters of the rock formations. The sources of hazards in civil engineering disciplines result essentially from undetected near-surface structures, such as cavities and/or inhomogeneities in the foundation geo-materials (Bremmer, 1999; Abdel-Hafez, 2004; Domenico and Sergio, 2009; Akintorinwa and Adesoji, 2009, and Araffa, 2010). Information related to the local soil conditions is vital for risk assessment and mitigation. Shallow seismic refraction and MASW are the ''work-horse'' of engineering geophysics, and have been widely applied to regolith mapping in geotechnical engineering (Whiteley, 1994).

The May 15th city is one of many new cities constructed around Greater Cairo, Egypt. It was established in 1978, and is located south of Greater Cairo, east of Helwan city (Fig. 1). It was constructed to solve the problem of insufficient accommodation. It includes many quarters, some of these quarters suffered from geotechnical problems, which appear as cracks of different sizes, specially at Quarter 27 causing the subsidence for some parts of the constructions and distribution of the clay layer and their effect by subsurface structures. Different authors tried to get the source of these geotechnical problems through geological, geophysical and geotechnical studies. Mohamed et al. (2012) investigated the southern part of the May 15th city using geological, geophysical and geotechnical data. They concluded that, the study area consists of four subsurface layers, the first layer is sand and clay (soil), and the second layer is composed of fractured limestone. The third layer is clayey marl and the fourth layer is marl. A number of normal faults trending NW-SE were delineated at different locations as shown in the geo-electrical, and geo-seismic cross sections. The limestone layer at shallow depths exhibits fractures and some buildings suffered oriented

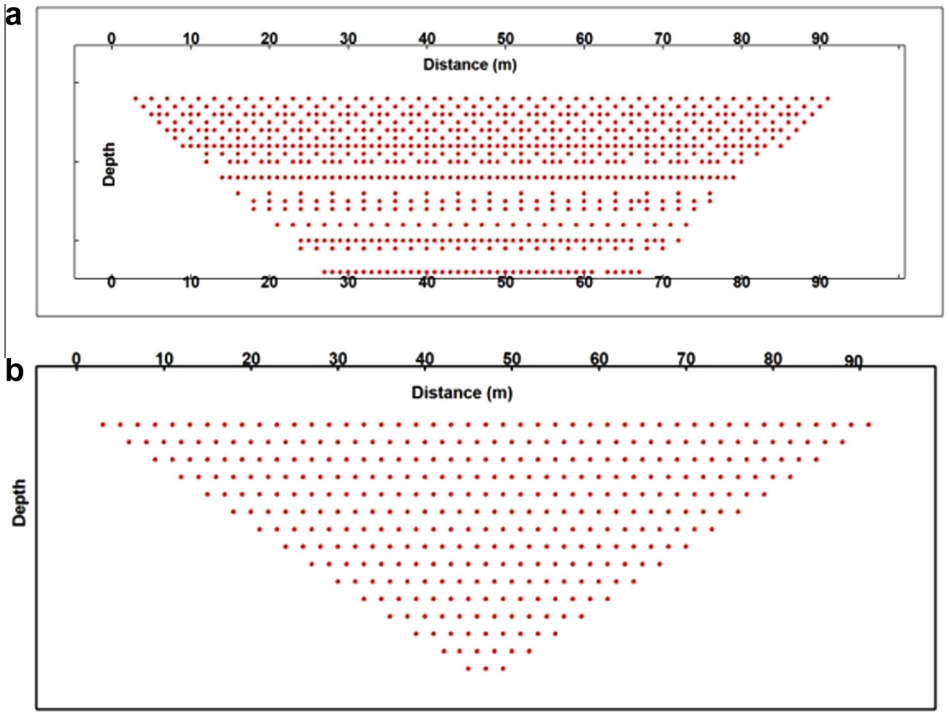

Fig. 3 Location map of measured points for (a) the dipole–dipole configuration and (b) the Wenner configuration.

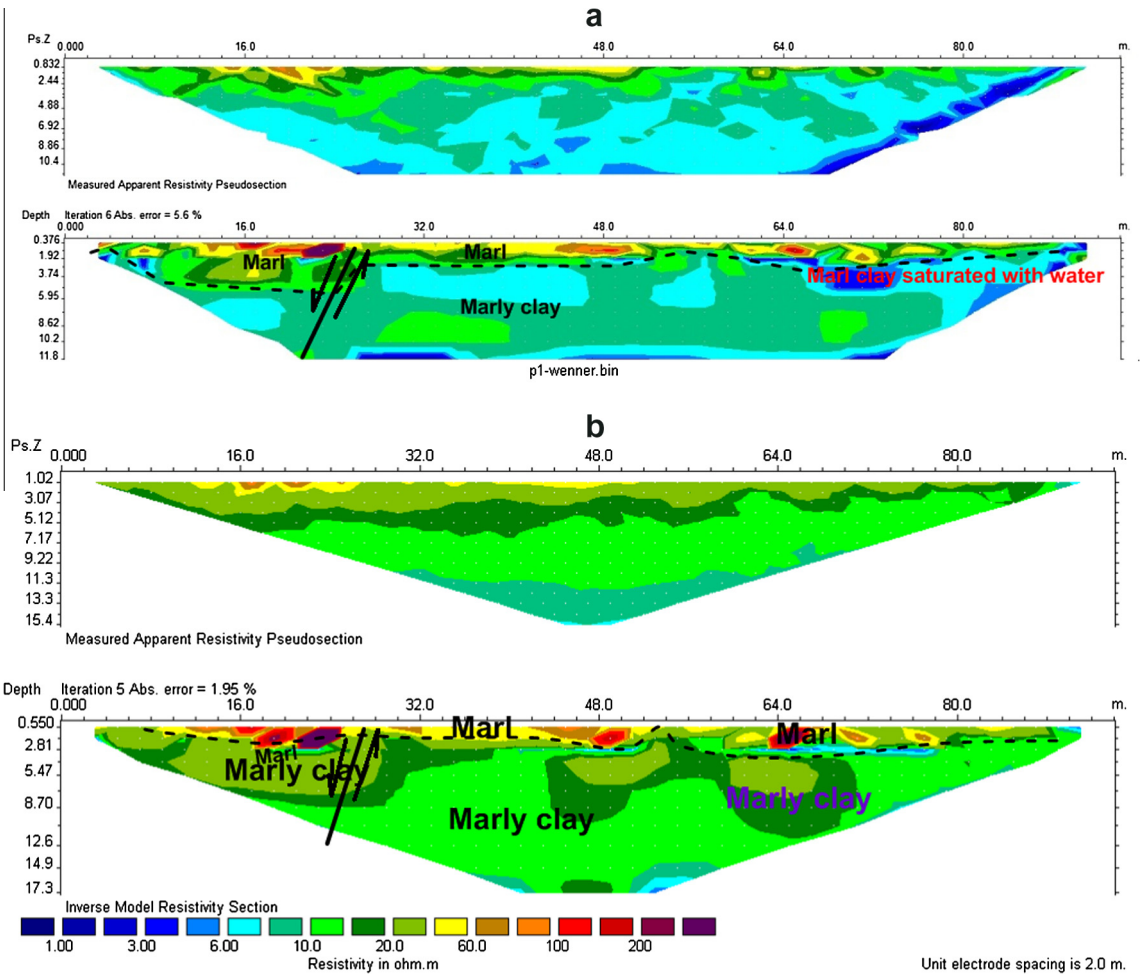

Fig. 4 The 2-D electrical resistivity section along profile P1–P1′, (a) dipole–dipole array and (b) Wenner array.

cracks, due to the effects of the fault elements, which dissect the study area. Atya et al. (2010) studied the near surface dynamics and its impact for foundation stability at Quarter 27 of the May 15th city. They concluded that the shallow surface of the ground is highly fractured producing a level of danger on the constructions and the block buildings at many sites of the Quarter. The move of the fracture center and its combination with the center of weight applied on the ground by the construction loads result in the change of the destruction resources which might lead to collapse, landslide, or divergence over the joints of the blocks.

2. Geology and Geomorphology of the study area

The study area is a part of the May 15th city, which is represented by Quarter 27. The study area consists of deposits of Pliocene, Upper, and Middle Eocene. The Pliocene deposits represented by wadi deposits, which is composed of compacted sandstone of medium to coarse grains. These deposits occupy the southwestern part of the May 15th city. The Upper Eocene deposits are represented by Wadi Garawi and Qurn Formations, while the Middle Eocene deposits are represented by Observatory Formation. Wadi Garawi Formation distributes at the south and southwestern parts of the May 15th city and consists of marl and marly limestone with clay intercalation at the upper part of the formation with thicknesses ranging from 50 to 80 m. Qurn Formation, which belongs to the Upper Eocene and covers most of the May 15th city, is composed of five units. The study area is dissected by two essential sets of faults trending NW-SE (Mohamed et al., 2012).

3. Methodology

3.1. Resistivity tool

3.1.1. Data acquisition

Electrical resistivity measurements are executed through applying Wenner and dipole–dipole configurations using SYSCAL-R2, as a resistivity-meter, which is fully automatic equipment designed for DC electrical exploration. The measurements are carried out in a fully automatic manner through the control of a microprocessor. Also, the SYSCAL-R2 unit can be a remote controlled through the serial link (reading of stored measurement points and control for the whole functions). It can also be connected to a network of intelligent nodes and thus be used as an automatic Multi-Electrode

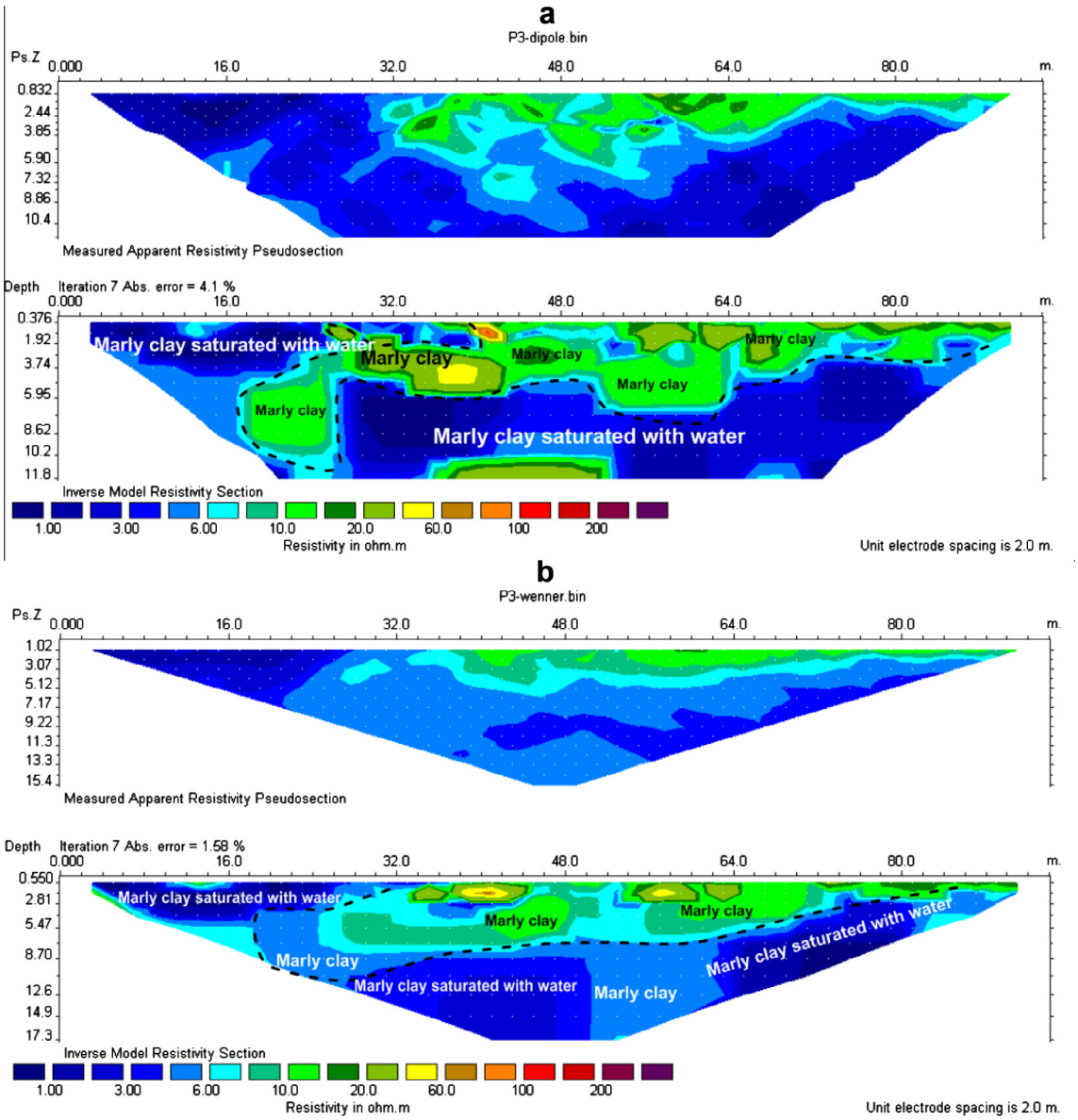

Fig. 5 The 2-D electrical resistivity section along the profile P3–P3′; (a) dipole–dipole array.

(ME) switching system array. Eight profiles have been measured with a spacing of two meters between the profiles (Fig. 2). The apparent resistivity value is given by:For Wenner configuration:

$$\rho_a = 2\pi aR \tag{1}$$

For dipole–dipole configuration:

$$\rho_a = 2\pi an(n+1)(n+2)R \tag{2}$$

where: R is the measured resistance, a is the spacing between the electrodes. The resistivity data were measured by using the automatic Multi-Electrode switching system of 48 nodes, where the data are automatically executed and stored in the storage memory of the instrument. The measurements were carried out at different levels which are function in the depth of penetration and electrode spacing (a) is equal to two meters. The Wenner levels (n) are ranging from 1 to 15 and in dipole–dipole n is ranging from 1 to 7. Eight Wenner profiles were measured in the study area with spreading length of 96 m for each profile. Each profile contains 360 measured points representing the fifteen levels. In addition to eight profiles of dipole–dipole were carried out at the same locations of Wenner profiles, in order to compare the results of the two techniques. In the dipole–dipole array, the electrode spacing is 2, 4 and 6 m respectively (Fig. 3). The RMS errors for all the measurements are ranging from 1.7 to 5 ohm m.

3.1.2. Data interpretation

The processing and interpretation of the obtained data have been done using commercial software for geo-electrical 2-D inversion (RES2DINV, 2001). Griffiths and Barker (1993) explain the theory and methodology of the routines applied in the software in detail. The 2-D model used by RES2DINV consists of a number of rectangular blocks. The arrangement of these blocks is loosely tied to the distribution of the data points in the pseudo-section. The depth of the bottom row

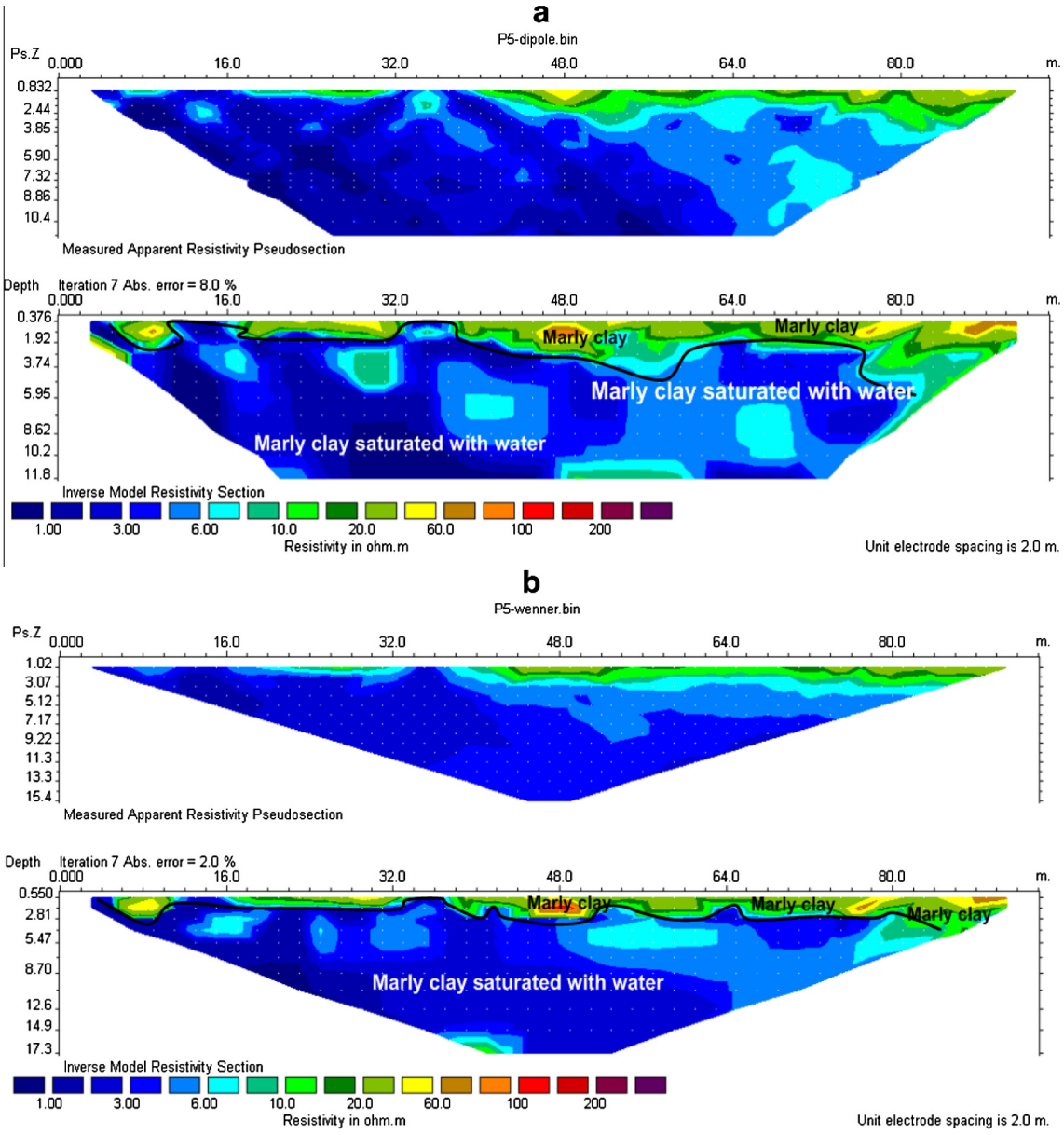

Fig. 6 The 2-D electrical resistivity section along the profile P5–P5′; (a) dipole–dipole array and (b) Wenner array.

of blocks is set to be approximately equal to the equivalent depth of investigation of the data points with the largest electrode spacing (Edwards, 1977).

In the present study, the obtained data have undergone several steps through RES2DINV software to be more smooth and clear for interpretation processes. For this purpose, two-dimensional (2-D) resistivity model of the acquired data has been automatically determined according to the expressive blocks and the distribution of the data points in the pseudo-section. The inversion sections of Wenner techniques more depth of penetration, about 17 m and for dipole–dipole sections (Figs. 4–6) are more resolution and the depth of penetration reaches 13 m. The inverted sections demonstrate that, the deduced subsurface section is classified into three main geo-electrical units. The first unit is fractured marl and limestone, which exhibits high resistivity values ranging from 40 to 300 ohm m. The second unit is corresponding to clayey marl of moderate resistivity values and the third unit is the deeper unit and exhibits very low resistivity values corresponding to clayey marl saturated with water.

Also, the results of interpretation of the obtained data for Wenner array are represented in the 3-D view to delineate the zones of very low resistivity values which are corresponding to clayey marl saturated with water and have direct effect on the constructions and may cause cracks and fractures (Fig. 7). This figure represents the slices at depths ranging from 0.38 to 2.79 m, which reveals the high resistivity values corresponding to marls at the southeastern and central parts of the study area (Fig. 7a). The northern part of the area shows very low resistivity values corresponding to marly clay saturated with water at depths ranging from 3.74 to 11.85 m (Fig. 7b and 7c). The constructions on this part of the area

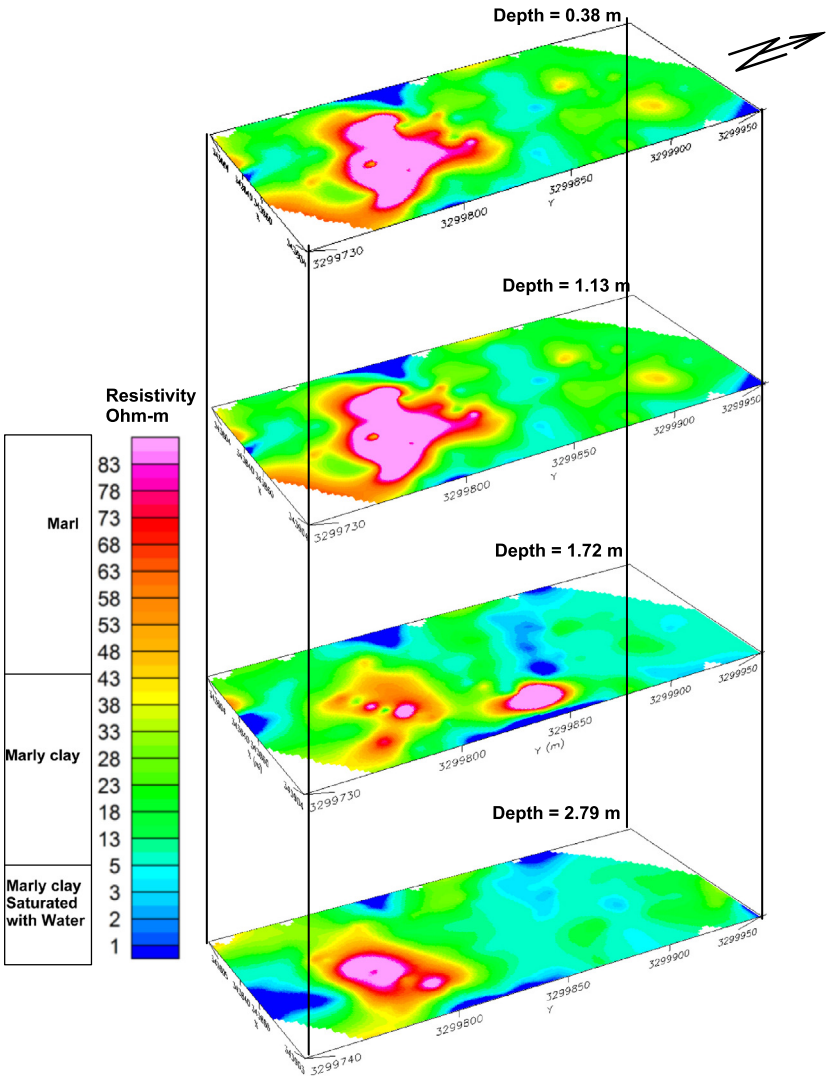

Fig. 7a The 3-D (tomography) resistivity view at depth slices from 0.38 to 2.79 m.

suffer from a lot of cracks and fractures due to this situation of subsurface geology.

3.2. Seismic tool

3.2.1. P-waves shallow seismic refraction

Nine shallow seismic refraction spreads for longitudinal waves (Fig. 8) were carried out to cover Quarter 27. The field survey was carried out using a seismograph model Strata View (of 1 ms sensitivity) manufactured by Geometrics Company (Underwood, 2007). The acoustic waves were generated by using a sledge hammer of 15 kg weigh as a seismic source. Forty-eight geophones for seismic spread (of 47 m spread length) were used with a spacing of 1 m for spreads S1 and S2, and geophone spacing of 2 m with spread length of 96 m for the rest (seven spreads). Five shots are carried out, the first shot is the normal one at 5 m before the first geophone, the second shot at the half distance between geophones 12–13, the third one is the midpoint between geophones 24–25, the fourth shot between geophones 36–37 and the last shot is the reverse one at 5 m after the last geophone. The data have been processed and interpreted using SIPT2 (RIMROCK, 1992), SeisRefa and SeisImager software packages. The interpretation of data is based on the iterative ray-tracing technique, in which the ray propagation will be simulated through a model (Scott, 1973). The results of the interpretation for 9 spreads reveal four layers, the first is surface layer composed of fragments of limestone and marl with P-wave velocity ranging from 0.3 to 0.35 km/s and of thickness less than 1 m. The second layer reveals low velocity ranging from 0.4 to 0.55 km/s and corresponding to fractured marl. The third layer reflects moderate velocity values ranging from 0.7 to 1.5 km/s, which is composed of marly clay. The fourth layer is composed of marly clay saturated with water and exhibits velocity values ranging from 1.8 to 2.2 km/s. Fig. 9 shows an example of the recorded seismograms of the profile S3–S3′. The time distance (T-D) curves and the geo-seismic depth sections are deduced (Figs. 10 and 11).

3.2.2. Multi-channel Analysis of Surface Waves (MASW)

Another technique to determine the shear wave velocities is applied using the surface waves. This is the most common type of Multi-channel Analysis of Surface Waves (MASW) survey

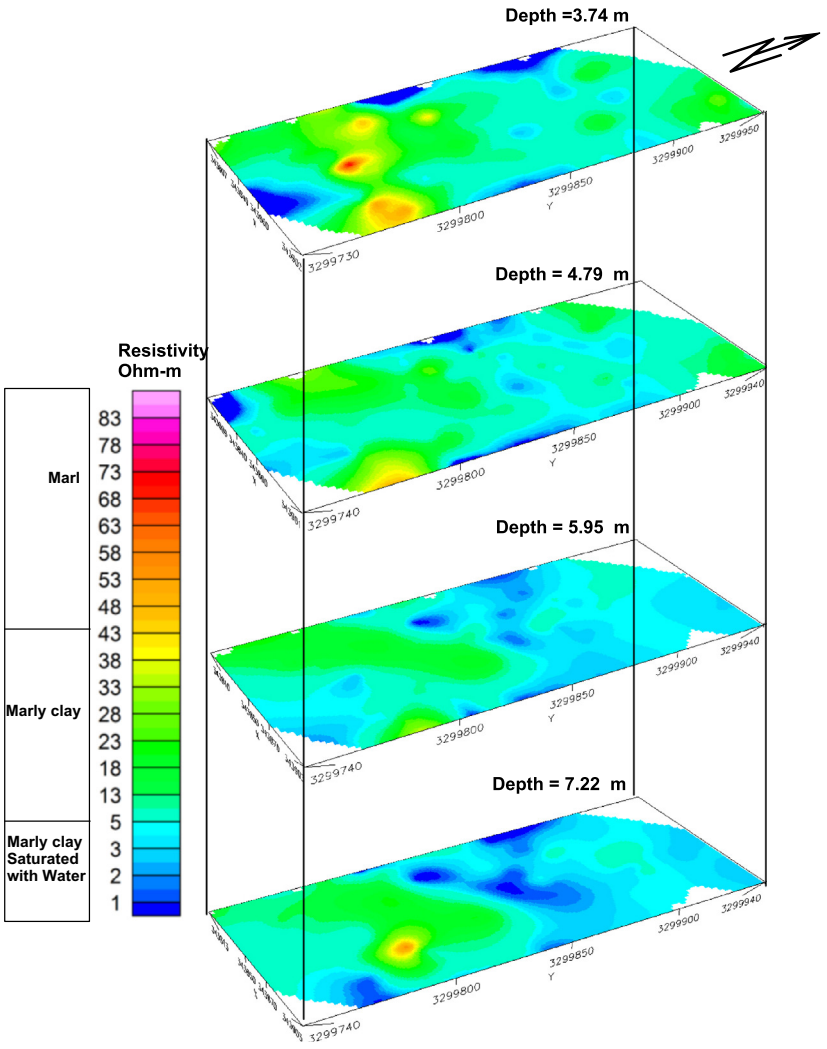

Fig. 7b The 3-D (tomography) resistivity view at depth slices from 3.74 to 7.22 m.

(Park et al., 1999). The maximum depth of investigation, that can be achieved, is usually in the range 10–30 m, but this can vary with sites and types of active sources used. A fairly heavy sledge hammer was used as a source in the active MASW survey. Stacking with multiple impacts can suppress ambient noise significantly and is therefore always recommended, specially, if the survey takes place in an urban area. Low-frequency (of 4.5 Hz) geophones are used. The length of the receiver spread is directly related to the longest wavelength that can be analyzed, which in turn determines the maximum depth of investigation. On the other hand, (minimum if uneven) receiver spacing is related to the shortest wavelength and therefore the shallowest resolvable depth of investigation. A one millisecond of sampling interval is most common with a 2-s total recording time (T = 2 s).

The MASW spreads were carried out along the same spreads of the P-wave shallow seismic refraction (Fig. 9) using 24 geophones. Each spread is of 46 m length. One shot was applied using a 15 kg sledge hammer at a distance of 5 m before the first geophone (1-D active MASW). The processing and interpretation are carried out using the SurfSeis-3 software package for 1-D MASW, passing through the following steps: surface wave imaging (overtone), constructing the dispersion curve as shown in Fig. 12, preparing the initial model (from the available boreholes and the P-wave model) and applying the inversion technique as shown in Fig. 13. The MASW technique is one of the seismic surveys for determining the shear wave velocity and consequently, evaluating the elastic condition (stiffness) of the ground for geotechnical engineering purposes.

3.2.3. The elastic moduli and geotechnical parameters

The obtained P- and S-wave velocities which are deduced from both the P-wave shallow seismic survey and the Multi-channel Analysis of Surface Waves (MASW) are used to evaluate the elastic moduli and geotechnical parameters.

The elastic moduli such as: density (Eq. (3)) (Gardner et al., 1974), Poisson's ratio (Eq. (4)) (Telford et al., 1976), Rigidity modulus (Eq. (5)), Young's modulus (Eq. (6)) and Bulk's modulus (Eq. (7)) are listed in Table 1.

$$\rho = 0.3 V_{\mathrm{p}}^{0.25} \tag{3}$$

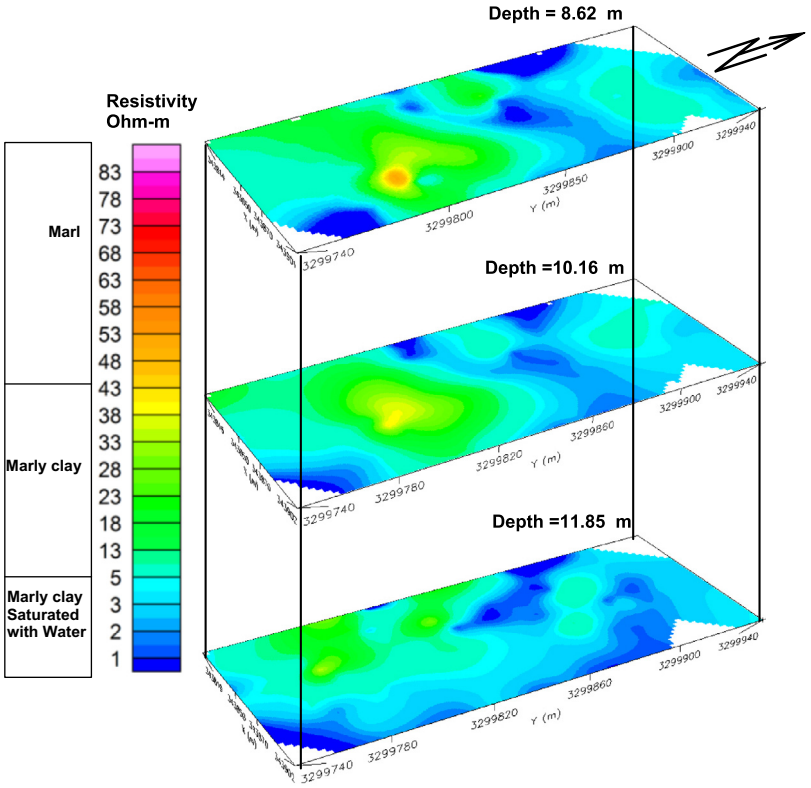

Fig. 7c The 3-D (tomography) resistivity view at depth slices from 8.62 to 11.85 m.

where: V_p is the P-wave velocity.

$$\sigma = ((V_p/V_s)^2 - 2)(2(V_p/V_s)^2 - 2) \quad (4)$$

where: V_s is the shear wave velocity.

$$\mu = V_s^2 \rho \quad (5)$$

$$Y = (1+\sigma)^2 \mu \quad (6)$$

$$B = (Y/(1-2\sigma)^{1/3}) \quad (7)$$

The geotechnical parameters such as: the *N*-value, bearing capacity and the site classes according to the weighting average of the shear wave velocity (V_s^{30}) down to 30 m depth (IBC, 2003) are evaluated as follows:

a. *N*-Value:

The *N*-value represents the geotechnical parameter SPT (Standard Penetration Test), which is defined as the resistance to penetration by normalized cylindrical bars under standard load, geophysically determined utilizing the modified Imai's formula (1976) by Stumpel et al. (1984) as follows (Eq. (8)):

$$V_s = 89.9 \cdot N^{0.341} \quad (8)$$

The *N*-value was originally adopted to investigate the status of cohesion-less deposits, and the low competent rocks reveal low *N*-value and vice versa.

b. Bearing capacity

In geotechnical engineering, the bearing capacity is known as the capacity of soil to support the loads applied to the ground. The bearing capacity of soil is the maximum average

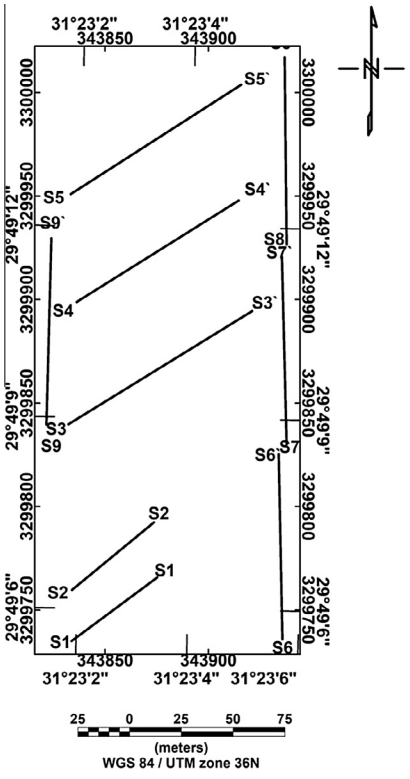

Fig. 8 Location map of the Shallow seismic refraction spreads.

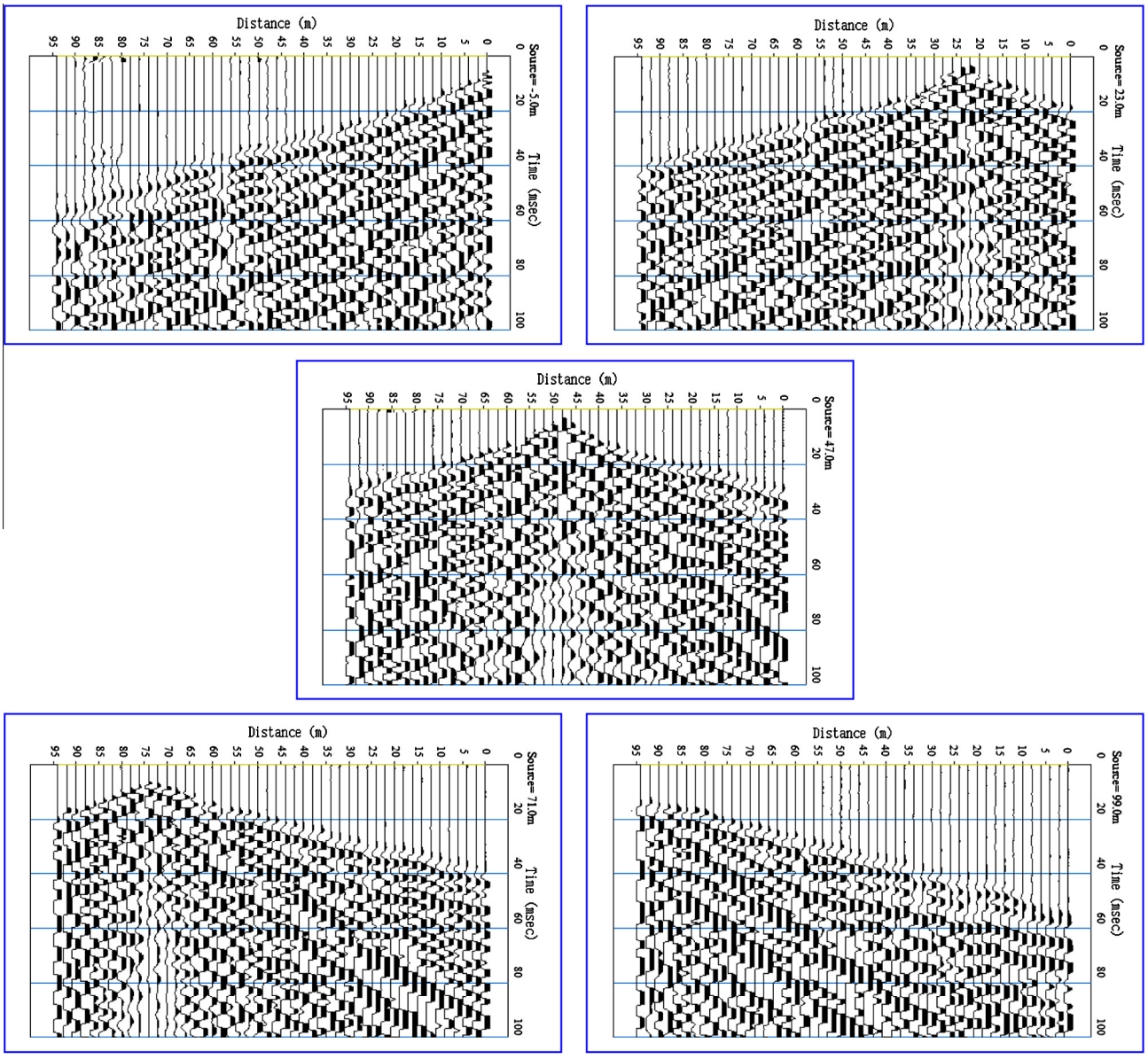

Fig. 9 The P-wave seismograms of the shallow seismic refraction survey of profile S7–S7′ as an example: the normal shot at −5 m (upper left panel), the inline shot at 23 m (upper right panel), the midpoint shot at 47 m (middle panel), the inline shot at 71 m (lower left panel) and the reverse shot at 99 m (lower right panel).

contact pressure between the foundation and the soil which should not produce shear failure in the soil.

The ultimate bearing capacity (Q_{ult}) provided by Parry (1977) is the theoretical maximum pressure which can be supported without failure (Eq. (9)).

The allowable bearing capacity (Q_{all}) is the maximum load to be considered to avoid sand liquefaction or shear failure, which should be taken into consideration during design purposes. It is the ultimate bearing capacity multiplied by a safe factor (Eq. (9)). Sometimes, on soft soil sites, large settlements may occur under loaded foundations without actual shear failure occurring; in such cases, the allowable bearing capacity is based on the maximum allowable settlement.

$$Q_{ult} = 30N = 10^{2.9322(\log V_s - 1.45)} \quad (9)$$

$$Q_{all} = Q_{ult}/F_s \quad (10)$$

where F_s is the safety factor ranging from 2 to 3 according to the type of lithology.

c. V_s^{30}

Ground motion is controlled by a number of variables, including the characteristic of the source, the propagation path and the near-surface geology. Elastic properties of near-surface materials and their effects on seismic wave propagation are very important in earthquake and civil engineering, and in environmental and earth science studies. The increase of amplitudes in soft sediments is one of the most important factors responsible for the amplification of earthquake motions. The amplification of seismic waves is closely linked with areas where a strong acoustic impedance is present, i.e., where layers

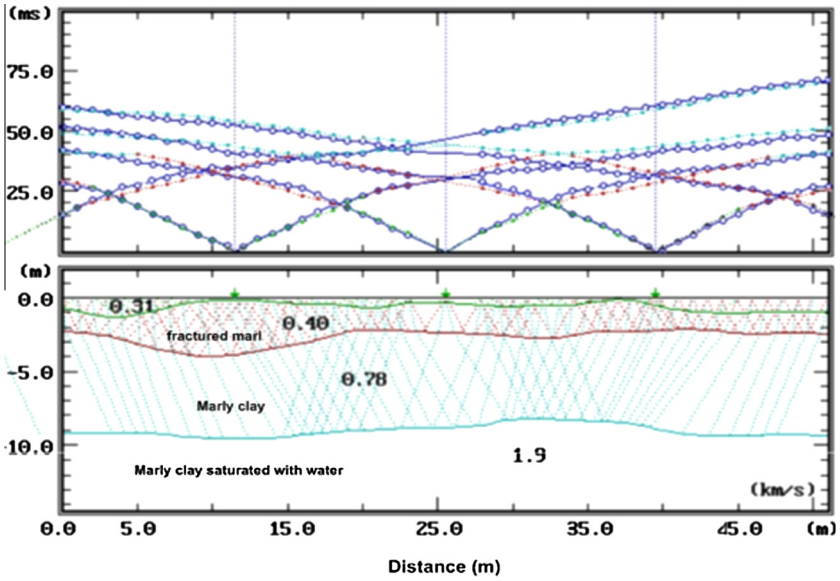

Fig. 10 The Time Distance (T-D) curves for the seismic profile S1–S1′ (upper panel) and the geo-seismic depth section and velocity model (lower panel) along S1–S1′.

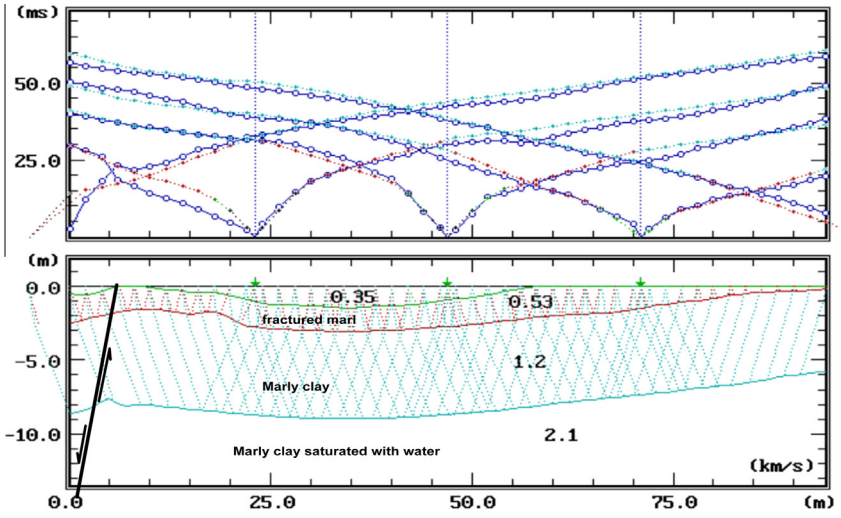

Fig. 11 The Time Distance (T-D) curves for the seismic profile S9–S9′ (upper panel) and the geo-seismic depth section and velocity model (lower panel) along S9–S9′.

of low seismic velocity overlie stiff soils or bedrock with a high seismic velocity. The amplification A is proportional to the reciprocal square root of the product of the shear wave velocity V_s and the density ρ of the investigated soil (Aki and Richards, 2002):

$$A \propto \frac{1}{\sqrt{V_s \rho}} \tag{11}$$

where: V_s is the shear wave velocity and ρ is the density of the investigated soil since density is, in general, relatively constant with depth, and the V_s profile better describes the local site conditions.

The average shear wave velocity of the upper 30 m (V_s^{30}) should be computed in accordance with the following expression:

$$V_s^{30} = \frac{30}{\sum_{i=1}^{N} \left(\frac{h_i}{c_i}\right)} \tag{12}$$

where: h_i and v_i denote the thickness (in meters) and shear-wave velocity (at a shear strain level of 10^{-5} or less) of the ith formation or layer, in a total of N, existing in the topmost 30 m. V_s^{30} was accepted for site classification in the International Building Code (IBC, 2003) as listed in Table 1.

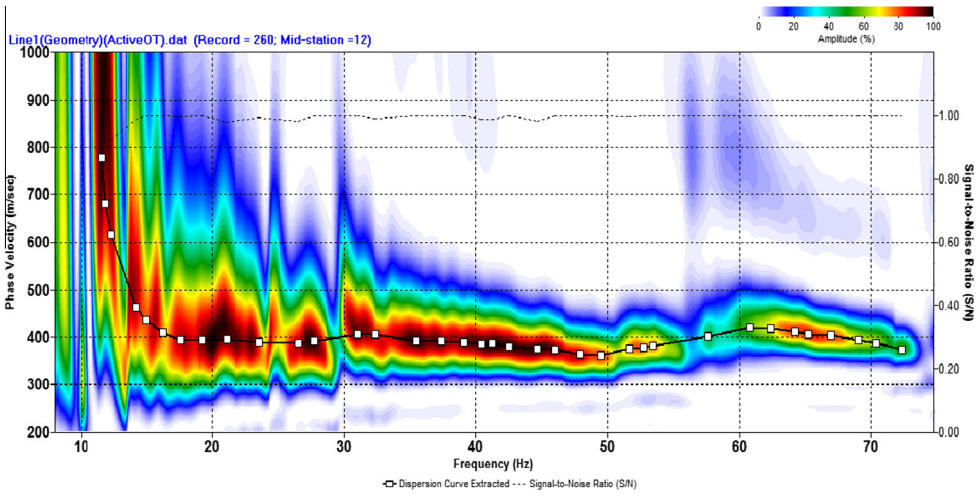

Fig. 12 The dispersion overtone (image) of the recorded surface waves and the dispersion curve with high S/N ratio at the profile S7–S7′.

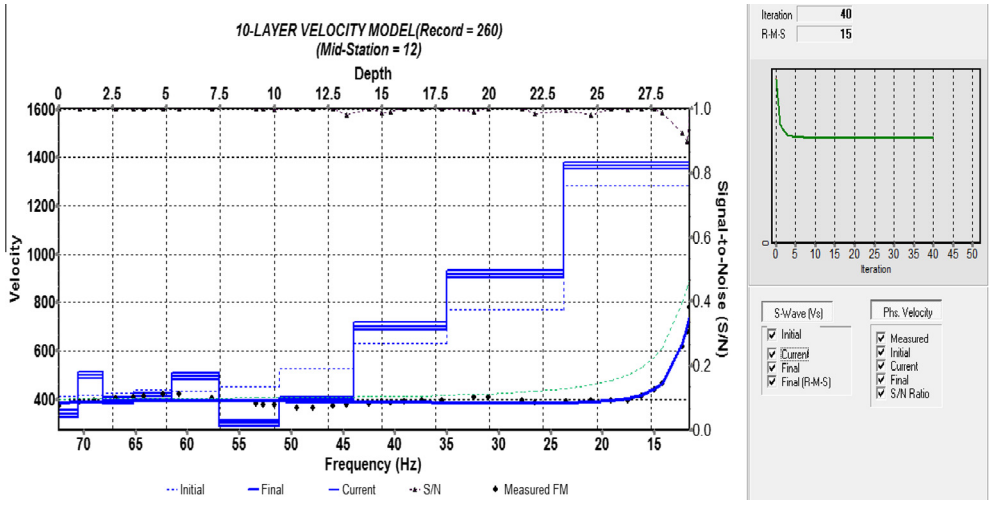

Fig. 13 The 1-D shear wave model deduced from the observed dispersion curve using the inversion technique at the profile S7–S7′.

Table 1 The site classification, according to the IBC code (2009).

Site class	Average shear wave velocity V_s^{30}	Remarks
A	$V_s^{30} > 1500$ (m/s)	Hard rock
B	$760 \leqslant V_s^{30} \leqslant 1500$ (m/s)	Rock
C	$360 \leqslant V_s^{30} \leqslant 760$ (m/s)	Very dense soil or soft rock
D	$180 \leqslant V_s^{30} \leqslant 360$ (m/s)	Stiff soil
E	$V_s^{30} < 180$ (m/s)	Soil
F	$V_s^{30} < 180$ (m/s)	Soil requiring site-specific evaluation

The elastic moduli and the geotechnical parameters using the mentioned empirical relations are obtained and listed in Table 2.

4. Discussion

The integration of geo-electrical and shallow seismic refraction data are used to define the properties and characteristics of the different subsurface layers and to delineate the structural elements which could have direct effects on the constructions in the Quarter 27, which is a part of the May 15th city. Geological study, which includes field work and geological descriptions at many observation points indicates that the study area consists of different geological units belong to different geological formations. The main formation in the study area is Qurn Formation which composed of five geological units, occupying almost the entire study area. Most of these units

Table 2 The elastic moduli and the geotechnical parameters at the interested area.

Profile	Layers	V_p (m/s)	V_s (m/s)	ρ (gm/cc)	σ	μ (dyn/cm)	Y (dyn/cm)	B (dyn/cm)	N-Value	Q_{ult} (kg/cm^2)	Q_{all} (kg/cm^2)	Class (m/s)	
												V_s^{30}	class
S1–S1′	1	310	175	1.30	0.27	4.0E+08	1.0E+09	7.2E+08	7.1	0.21	0.11	712	C
	2	400	215	1.39	0.30	6.4E+08	1.7E+09	1.4E+09	12.9	0.40	0.20		
	3	780	450	1.64	0.25	3.3E+09	8.3E+09	5.5E+09	> 50	3.40	1.70		
	4	1900	1120	2.05	0.23	2.6E+10	6.3E+10	4.0E+10	> 50	48.9	24.4		
S2–S2′	1	280	165	1.27	0.23	3.5E+08	8.5E+08	5.3E+08	5.9	0.18	0.09	539	C
	2	440	225	1.42	0.32	7.2E+08	1.9E+09	1.8E+09	14.7	0.40	0.20		
	3	970	495	1.73	0.32	4.2E+09	1.1E+10	1.1E+10	> 50	4.50	2.20		
	4	1900	1120	2.05	0.23	2.6E+10	6.3E+10	4.0E+10	> 50	48.9	24.4		
S3–S3′	1	280	165	1.27	0.23	3.5E+08	8.5E+08	5.3E+08	5.9	0.18	0.09	319	D
	2	1300	720	1.86	0.28	9.6E+09	2.5E+10	1.9E+10	> 50	13.4	6.70		
	3	2000	1020	2.07	0.32	2.2E+10	5.7E+10	5.4E+10	> 50	37.1	18.6		
	4	3600	1835	2.40	0.32	8.1E+10	2.1E+11	2.0E+11	> 50	207.8	103.9		
S4–S4′	1	280	165	1.27	0.23	3.5E+08	8.5E+08	5.3E+08	5.9	0.18	0.09	398	C
	2	510	310	1.47	0.21	1.4E+09	3.4E+09	1.9E+09	> 50	1.10	0.60		
	3	1100	745	1.79	0.08	9.9E+09	2.1E+10	8.4E+09	> 50	14.8	7.40		
	4	2300	1340	2.15	0.24	3.9E+09	9.6E+10	6.2E+10	> 50	82.7	41.3		
S5–S5′	1	400	210	1.39	0.31	6.1E+09	1.6E+10	1.4E+09	12.0	0.36	0.18	437	C
	2	1100	650	1.79	0.23	7.5E+09	1.9E+10	1.2E+10	> 50	9.90	5.00		
	3	1800	950	2.02	0.31	1.8E+09	4.8E+10	4.1E+10	> 50	30.1	15.1		
	4	3000	1650	2.29	0.28	6.2E+10	1.6E+11	1.2E+11	> 50	152.1	76.1		
S6–S6′	1	310	175	1.30	0.27	4.0E+08	1.0E+09	7.2E+08	7.1	0.21	0.11	424	C
	2	620	315	1.55	0.33	1.5E+09	4.1E+09	3.9E+09	39.5	1.20	0.60		
	3	1200	640	1.82	0.30	7.5E+09	1.9E+10	1.6E+10	> 50	9.50	4.70		
	4	2500	1375	2.19	0.29	4.1E+10	1.1E+11	8.2E+10	> 50	88.2	44.1		
S7–S7′	1	330	165	1.32	0.27	4.5E+08	1.2E+09	8.4E+08	8.3	0.25	0.12	313	D
	2	730	320	1.61	0.38	1.7E+09	4.6E+09	6.4E+09	41.4	1.20	0.60		
	3	1500	820	1.93	0.29	1.3E+10	3.3E+10	2.6E+10	> 50	19.6	9.80		
	4	2500	1375	2.19	0.28	4.1E+10	1.1E+11	8.2E+10	> 50	89.1	44.6		
S8–S8′	1	350	195	1.34	0.27	5.1E+08	1.3E+09	9.6E+08	9.7	0.29	0.15	370	C
	2	1200	590	1.82	0.34	6.4E+09	1.7E+10	1.8E+10	> 50	7.50	3.70		
	3	1700	765	1.99	0.37	1.2E+10	3.2E+10	4.2E+10	> 50	16.0	8.00		
	4	2600	1390	2.21	0.30	4.3E+10	1.1E+11	9.3E+10	> 50	92.0	46.0		
S9–S9′	1	350	200	1.34	0.26	5.4E+08	1.4E+09	1.4E+09	10.4	0.31	0.16	380	C
	2	440	260	1.42	0.23	9.6E+08	2.4E+09	2.4E+09	22.5	0.70	0.30		
	3	1000	580	1.74	0.25	5.9E+09	1.5E+10	1.5E+10	> 50	7.10	3.50		
	4	2100	1200	2.10	0.26	3.0E+10	7.6E+10	7.6E+10	> 50	59.8	29.9		

consist of marl intercalated with clay. This marly clay represents the main geotechnical problem. Two sets of faults trending NW-SE were investigated through detailed field geology at the area. The geo-electrical data which include Electric Resistivity Tomography (ERT) represented by dipole–dipole and Wenner sections indicate that, the study area consists of different geologic units according to the resistivity values, where the inversion of 2-D resistivity data and 3-D representation indicate that the subsurface section consists of different geologic units such as fragments of limestone, marl and marly clay where these units coincident with the geologic description. Also, shallow seismic refraction interpretation for P-waves and surface waves reveal four layers, the first as a surface layer is composed of fragments of limestone and marl, the second layer reveals fractured marl, the third layer reflects marly clay. The fourth layer is composed of marly clay saturated with water. The normal faults which dissect the Quarter 27 as shown in the geological map appear in two resistivity sections along the profiles P1–P1′ and P3–P3′ (Figs 4 and 5). The 3-D representation reflects these faults at shallow depths (Fig. 7a). In addition, these faults dissect the geo-seismic section along spread number S9–S9′. The marly clay layer is saturated with water. The normal faults, that dissect Quarter 27 cause cracks and fractures for most buildings of the Quarter, specially at building numbers 40 and 41. The presence of clay and water leads to weakening of the soil layer which is obvious in the geotechnical parameters as well as the site classes which reflect sites of class D and the lower limit of class C.

5. Conclusion

From the integrated interpretation for the geophysical data at the Quarter 27 in the May 15th city, we can conclude that, the study area consists of four subsurface layers, the first layer is the fragment of marl and limestone, marl, marly clay and marly clay saturated with water. A normal fault trending NW-SE is delineated at different locations as shown in the geo-electrical and geo-seismic cross-sections. The marl layer at shallow depths exhibits fractures. Some buildings suffered oriented cracks and fractures due to geotechnical problems for the subsurface situation of marly clay saturated with water and normal fault which dissects the Quarter 27.

References

Abdel-Hafez, T., 2004. Geophysical and Geotechnical Studies in Pharaonic and Urban Egypt (Ph.D thesis). Bern University, Germany, pp. 111.

Aki, K., Richards, P.G., 2002. Quantitative Seismology, second ed. University Science Books, 700.

Akintorinwa, O.J., Adesoji, J.I., 2009. Application of geophysical and geotechnical investigations in engineering site evaluation. Int. J. Phys. Sci. 4 (8), 443–454.

Araffa, S.A.S., 2010. Geophysical investigation for shallow subsurface geotechnical problems of Mokattam area, Cairo, Egypt. Environ. Earth Sci. J. 59, 1195–2207.

Atya, M., Khachay, O.A., Soliman, M., Khachay, O.Y., Khalil, A., Gaballah, M., Shaaban, F., El-Hemali, I., 2010. CSEM Imaging of the near surface dynamics and its impact for foundation stability at Quarter 27, 15th of May City, Helwan, Egypt. Earth Sci. Res..

Bremmer, C.N., 1999. Developments in geomechanical research for infrastructural projects. In: 12th European Conference on Soil Mechanic and Geotechnical Engineering: Geotechniek, Special Issue, pp. 52–55.

Domenico, P., Sergio, M., 2009. Geophysical tomography in engineering geological applications: A mini-review with examples. Open Geol. J. 3, 30–38.

Edwards, L.S., 1977. A modified pseudosection for resistivity and induced polarization. Geophysics 42, 1020–1036.

Gardner, G.H.F., Gardner, L.W., Gregory, A.R., 1974. Formation velocity and density – The diagnostic basics for stratigraphic traps. Geophysics 39, 770–780.

Griffiths, D.H., Barker, R.D., 1993. Two-dimensional resistivity imaging and modeling in areas of complex geology. J. Appl. Geophys. 29.

IBC, 2003. International Building Code: Site classification using the average shear wave velocity in the upper 30 m thickness. Section 1615.1.5, Equations 16–22 and 16–44.

Imai, T., Fumoto, H., Yokota, K., 1976. P- and S- wave velocities in subsurface layer of ground in Japan. Urawa Research Institute, Tokyo.

Klimis, N.S., Papazachos, C.B., Efremidis, Ch.F., 1999. Determination of the behavior of a sedimentary rock mass: comparison of measured static and dynamic properties. In: Proc. 9th Int. Conf. on Rock Mechanics (Paris, France).

Luna, R., Jadi, H., 2000. Determination of dynamic soil properties using geophysical methods. In: Proc. 1st Int. Conf. on the Application of Geophysical and NDT Methodologies to Transportation Facilities and Infrastructure Geophysics (Federal Highway Administration, Saint Louis, MO), vol. 3. pp 1–15.

Mohamed, A.M.E., Sultan, S.A., Mohamed, N.I., 2012. Delineation of near-surface structure in the southern part of the city of 15th May Cairo, Egypt using geological, geophysical and geotechnical techniques. Pure Appl. Geophys. 169, 1641–1654.

Othman, A.A.A., 2005. Construed geotechnical characteristics of foundation beds by seismic measurements. J. Geophys. Eng. 2, 126–138.

Park, C.B., Miller, R.D., Xia, J., 1999. Multichannel Analysis of Surface Waves (MASW). Geophysics 64.

Parry, R.H.G., 1977. Estimating bearing capacity of sand from SPT values. JGED ASCE 103 (Gt. 9), 1014–1043.

RES2DINV ver. 3.4, 2001. Rapid 2-D resistivity & IP inversion using the least-squares method, Geoelectric Imaging 2-D & 3D, Geotomo software (http://www.Geoelectric.com).

RIMROCK Geophysics, 1992. SIPT2 Refraction Processing Software, Version 3.2, Boulder, Colorado.

Savvaidis, A., Tsokas, G., Soupios, P., Vargemezis, G., Manakou, M., Tsourlos, P., Fikos, I., 1999. Geophysical prospecting in the Krousovitis dam (N Greece) by seismic and resistivity geophysical methods. J. Balkan Geophys. Soc. 2, 128–139.

Scott, J., 1973. Seismic refraction modeling by computer. Geophysics 38 (2), 271–284.

Soupios, P., Papazachos, C.B., Vargemezis, G., Savvaidis. A., 2006. In situ geophysical investigation to evaluate dynamic soil properties at the Ilarionas Dam, Northern Greece. In: Proc. 2nd Int. Conf. Advances in Mineral Resources Management and Environmental Geotechnology (Hania, Crete, Greece, 25–27 September 2006) (Heliotopos Conferences). pp. 149–56.

Stumpel, H., Kaehler, S., Meissner, R., Milkeret, B., 1984. The use of seismic shear waves and compressional waves for lithological problems of shallow sediments. Geophys. Prospect. 32, 662–675.

Telford, W.M., Geldart, L.P., Sheriff, R.E., Keys, D.A., 1976. Applied Geophysics. Cambridge University Press, 860 p.

Venkateswara, V.R., Srinivasa, R., Prakasa, R.B.S., Koteswara, R.P., 2004. Bedrock investigation by seismic refraction method – A case study. J. Ind. Geophys. Union 8, 223–228.

Whiteley, R.J., 1994. Seismic refraction testing – A tutorial. In: Woods, R.D. (Ed.), Geophysical Characterization of Sites. Oxford & IBH Publishing, pp. 45–47.

Underwood, D., 2007. Near-Surface Seismic Refraction Surveying Field Methods. Geometrics Inc.